Journal of ELECTRONIC MATERIALS, Vol. 48, No. 1, 2019
https://doi.org/10.1007/s11664-018-6752-1

Enhanced Gas-Sensing Response of Zinc Oxide Nanorods Synthesized via Hydrothermal Route for Nitrogen Dioxide Gas

S.A. VANALAKAR,[1,2,5] M.G. GANG,[2] V.L. PATIL,[1] T.D. DONGALE,[3] P.S. PATIL,[4] and J.H. KIM[2,6]

1.—Department of Physics, Karmaveer Hire Arts, Science, Commerce and Education College, Gargoti 416-009, India. 2.—Department of Materials Science and Engineering, Chonnam National University, Gwangju 500-757, Korea. 3.—School of Nanoscience and Biotechnology, Shivaji University, Kolhapur 416-004, India. 4.—Department of Physics, Shivaji University, Kolhapur 416-009, India. 5.—e-mail: sharad.vanalakar@gmail.com. 6.—e-mail: jinhyeok@chonnam.ac.kr

In recent years, advanced material processing techniques have allowed scientists to research and document the properties of nanostructured metal oxides. One such material system, zinc oxide (ZnO), has emerged as a favorable option for a multitude of applications. In this study, thin films of ZnO with nanorod-like architectures were hydrothermally formed on a glass substrate and their physical and chemical properties were thoroughly characterized. X-ray diffraction confirmed the wurtzite structure and a scanning electron microscope was used to verify the vertical alignment of the rods. Defects due to the high oxygen vacancy concentration were revealed through photoluminescence studies. The high surface area of the nanorods works in conjunction with these defects and an optimal inter-rod spacing creates conditions for effective gas adsorption and diffusion. With this in mind, the nanorods were used to fabricate a gas sensor which demonstrated excellent NO_2 sensitivity and selectivity at a relatively low operating temperature.

Key words: ZnO, nanorod, thin film, hydrothermal route, NO_2 gas sensor

INTRODUCTION

Environmental pollution has forced humanity to develop simple, reliable gas sensors to detect harmful, flammable, and explosive gases.[1–4] Nitrogen dioxide (NO_2) is one such environmentally hazardous gas. NO_2 is one byproduct of combustion in factories, exhaust of motor vehicles, and chemical and thermal power plants.[2] Excess NO_2 gas leads to the formation of ozone, smog, and nitric acid rain. In addition, high levels of NO_2 gas have been shown to decrease lung capacity and cause an upsurge in respiratory problems.[3] Therefore, there is need for sensitive, selective, and low-concentration level detection of NO_2 gas. To this end, metal oxides such as zinc oxide (ZnO), tin oxide (SnO_2), indium oxide (In_2O_3), tungsten oxide (WO_3), etc. have been proven to be strong candidates for simplistic and economical gas-sensing materials due to their low cost, compact size, flexibility, high gas-sensing activities, and the simplicity of their use.[5–10] Additionally, the semiconducting metal oxide gas sensors consist of simple components such as a sensing element, signal converter, and portable electronic devices. ZnO in particular has proven to be one of the most promising materials in sensor technology due to its excellent sensitivity, selectivity, and simple sensing operations. Moreover, the low-cost and environmentally benign components of ZnO as well as its higher exciton binding energy and band gap have been extensively explored for multiple practices such as gas sensors, photo-catalytic dye degradation, solar cell materials, etc.[11–14] In the literature, nanostructured ZnO with a wide variety of morphologies including needles, wires, fibers, rods, belts, tubes, flowers, particles, films, sheets, and plates has been studied extensively and used in gas-sensing applications.[15–17] Of these various

(Received March 17, 2018; accepted October 22, 2018; published online October 30, 2018)

morphologies, the nanorod, or wire-like, morphologies offer a high surface-to-volume ratio, maximum number of active sites at the surface, and good charge transfer and carrier mobility.[18] Various techniques have been used to deposit ZnO nanorods including chemical bath deposition, reflux, hydrothermal, and solvothermal techniques. Of these methods, the hydrothermal route offers numerous advantages such as simpler procedure and assembly, eco-friendly nature, low cost, and ability to fabricate free-standing nanostructures with various morphologies.[19–21] In addition, the ability to control the growth of the material by varying the temperature, pressure, and time of synthesis is another advantage of the hydrothermal method. Thus, that method was chosen for use in this study.

Here, we explore gas-sensing properties of a ZnO nanorod thin film-based sensor with regard to NO_2. Before the sensing properties could be studied, the ZnO thin films were prepared using a simplistic hydrothermal method with different concentrations of a zinc ion solution. The structural, surface morphology, and optical properties of the ZnO thin films were studied using x-ray diffraction (XRD), field emission scanning electron microscopy (FESEM), and room-temperature photoluminescence (PL) spectroscopy. The synthesized ZnO thin films show a sensitive and selective detection of NO_2 gas at relatively low operating temperatures.

METHOD AND MATERIALS

Zinc nitrate [$Zn(NO)_3{\cdot}6H_2O$], ammonium hydroxide (NH_4OH), and tri-sodium citrate ($C_6H_5Na_3O_7{\cdot}2H_2O$) of analytical grade were purchased from Sigma-Aldrich and used without further purification. The synthesis of ZnO nanorod thin films in our study was reported earlier in the literature.[22,23] In short, at first, a 100-nm-thick ZnO seed layer was deposited over soda-lime glass substrate by using the radiofrequency (RF) sputtering method. Then, the seed layer of ZnO was dipped vertically in a Teflon-coated stainless-steel autoclave containing the precursor solution. Typically, the precursor solution contains $Zn(NO)_3$ in different concentrations, such as 0.2 g, 0.3 g, 0.4 g, and 0.5 g in 48 ml of deionized water. The 1.6 ml of NH_4OH solution was used to maintain the pH of the solution at around 11. An equal amount of trisodium citrate was used as a complexing agent. Then, the sealed autoclave was placed in an oven at 80°C for 90 min, and after completion of the reaction, the substrates were removed, rinsed with deionized water, and dried at room temperature. Figure 1 shows the experimental setup used in our laboratory. The ZnO thin film samples prepared for different zinc nitrate such as 0.2 g, 0.3 g, 0.4 g, and 0.5 g in 48 ml of deionized water are denoted as ZnO-a, ZnO-b, ZnO-c, and ZnO-d, respectively.

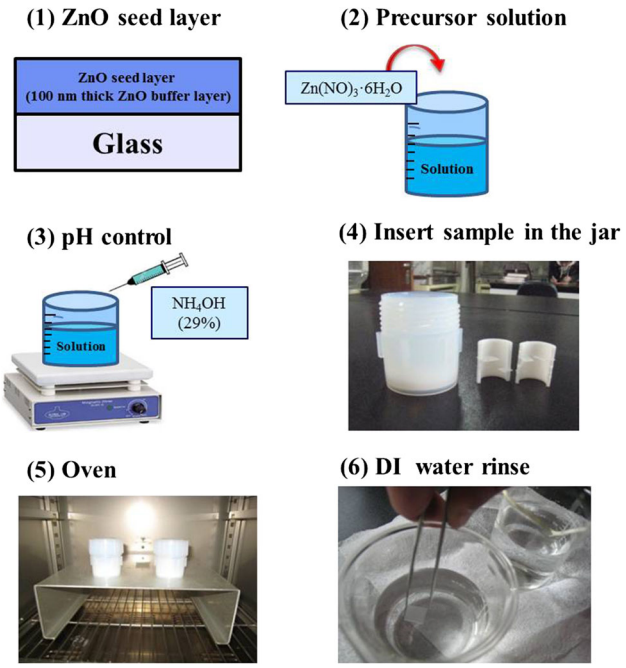

Fig. 1. Schematic representation of the experimental details used in our study. The steps involved in the experiments were: (1) growth of seed layer, (2 and 3) preparation of precursor solution and control of pH of the solution, (4) insertion of the sample in solution in a jar, and (5 and 6) deposition and washing of film with deionized water.

The structural properties of the as-synthesized ZnO thin films were studied using a high-resolution x-ray diffractometer with Ni-filtered Cu-$K\alpha 1$ radiation of 1.54056 Å (X'pert PRO, Philips, Eindhoven, Netherlands). The surface morphology of the as-synthesized ZnO thin films was recorded via field emission scanning electron microscopy (FESEM; model S-4700, Hitachi, Japan). The PL spectra of the ZnO thin film samples were recorded using a PL spectrophotometer (PI-Max3, Princeton Instruments, USA). To study the gas-sensing properties of ZnO nanorods, the home-built, computer-controlled static gas-sensing system with a Keithely 6514 electrometer was used. The gas-sensing system consisted of an air-tight stainless-steel test chamber having volume capacity of 250 cc with the provision of a gas inlet/outlet, and a flat heating plate with a temperature controller. Initially, the thin film sample was preheated at a desired temperature using a hot plate and monitored by the temperature controller. During the measurement, the film area for all ZnO thin films was kept constant and a known amount of gas was injected into the system to measure the change in the electrical resistance of the films with respect to the variation in the NO_2 gas concentrations at different operating temperatures. The gas response (S [%]) is calculated using the following equation:

$$S(\%) = \frac{R_g - R_a}{R_a} \times 100 \qquad (1)$$

where R_a is the resistance of the film in the air and R_g is the resistance of the film after gas exposure.

RESULTS AND DISCUSSION

Figure 2 depicts the XRD pattern of all ZnO film samples synthesized via the hydrothermal route. The diffraction peaks observed in Fig. 2 can be indexed to the hexagonal wurtzite ZnO, consistent with the JCPDS card no. 36-1451. The main intense (002) peak indicates the vertical growth of ZnO, which is perpendicular to the substrate. Moreover, with the increase in zinc nitrate concentration, the intensity of the (002) peak increases further. The increased peak intensity strongly suggests the growth of ZnO preferentially in one dimension: along the c-axis.[24] In addition, the diffraction peaks are narrow and intense which indicates the high crystallinity of the as-synthesized ZnO samples. Interestingly, the XRD pattern shows slight enhancement of the (100) peak intensity with the increase in the zinc nitrate concentration.

Figure 3 shows the FESEM images of ZnO thin films synthesized by hydrothermal route with different concentrations of the zinc nitrate solution. As observed in Fig. 3, all ZnO thin film samples contain vertically aligned nanorods. In addition, the nanorods become denser and their size grows larger as the amount of the zinc nitrate in the bath solution increases. However, they become slightly shorter for the sample ZnO-d as compared to its preceding counterpart. The decrease in the rod length is partially compensated for by the increase in the rod width. The increase in the zinc nitrate concentration may be responsible for the higher rate of dissolution of the (002) facet up to a certain limit. A further increase in the zinc nitrate concentration enhances the width of the nanorod on account of its length. For the samples ZnO-b and ZnO-c, the spacing between adjacent nanorods was seen equally distributed and for sample ZnO-d, the spacing was very low and it looks like the nanorods overlap. The FESEM images of all the ZnO thin films are consistent with the XRD patterns. Meanwhile, the linear nanorods with adequate inter-rod distance provide effective space for gas adsorption/desorption.

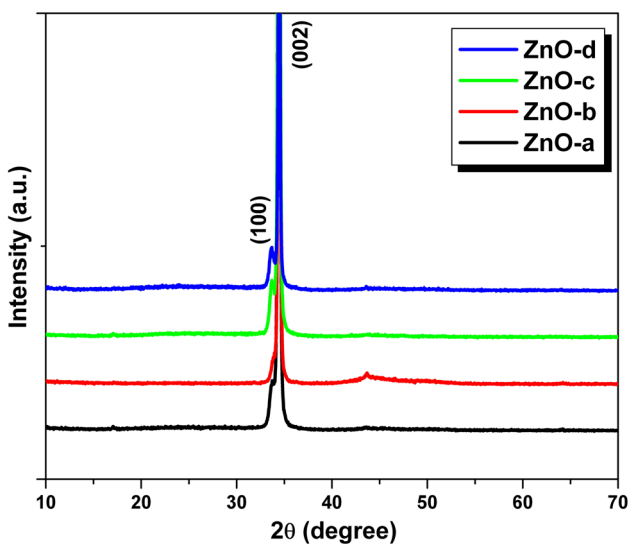

Fig. 2. The XRD patterns of hydrothermally grown ZnO thin films samples.

The inhabitant defects such as oxygen vacancies and doping impurities allied with metal oxides are the vital features of the gas-sensing properties, as gas sensing is a surface phenomenon and the oxygen vacancies induce a large number of electron donors on the surface of ZnO structures.[25–30] Moreover, the higher oxygen vacancies present in the ZnO sample form a thicker electron depletion layer due to the large number of electrons captured from the conduction band of ZnO. Such a thick electron depletion layer boosts the gas-sensing performance of ZnO thin films. PL spectroscopy is an effective way to study the defects present in the metal oxide semiconductors.[26,27] Figure 4 shows the room-temperature PL spectra of all ZnO nanorod samples. The broad PL peak for all ZnO samples appears at $\sim$ 600 nm corresponding to the visible region. This PL peak in the visible region is attributed to the deep-level emissions and is ascribed to the presence of oxygen vacancies, interstitial sites, and defects.[28–30] In addition, the intensity of the PL peaks in our study is found to be different for different ZnO samples. In general, the PL peak intensity indicates the presence of defects and/or oxygen vacancies; maximizing the PL peak intensity indicates maximum defects, as the PL peak intensity increases further from sample ZnO-a to sample ZnO-c. Therefore, the defect level increased from sample ZnO-a to sample ZnO-c. Meanwhile, sample ZnO-d shows slightly lower PL peak intensity compared to sample ZnO-c.

The operating temperature is the most important influencing factor of gas response of a semiconductor metal oxide gas sensor. So, to determine the optimal operating temperature, we performed a gas-sensing test for all the ZnO samples at an NO_2 gas concentration of 100 ppm. Figure 5 shows the variation of gas response for all the ZnO thin film samples as a function of the operating temperature. In the range of working temperatures, the gas response of all the ZnO thin film samples increases further incrementally in the working temperature and then decreases beyond the operating temperature of 150°C. The maximum gas response is observed at 150°C for all ZnO thin film samples, which is considered as the optimum operating temperature in our study. The lower gas response in the operating temperature range of 100 to 150°C is due to the weak chemical reactions at the surface caused by insufficient thermal energy, and poorer gas response at higher temperature is ascribed to less availability of NO_2 gas due to its conversion into

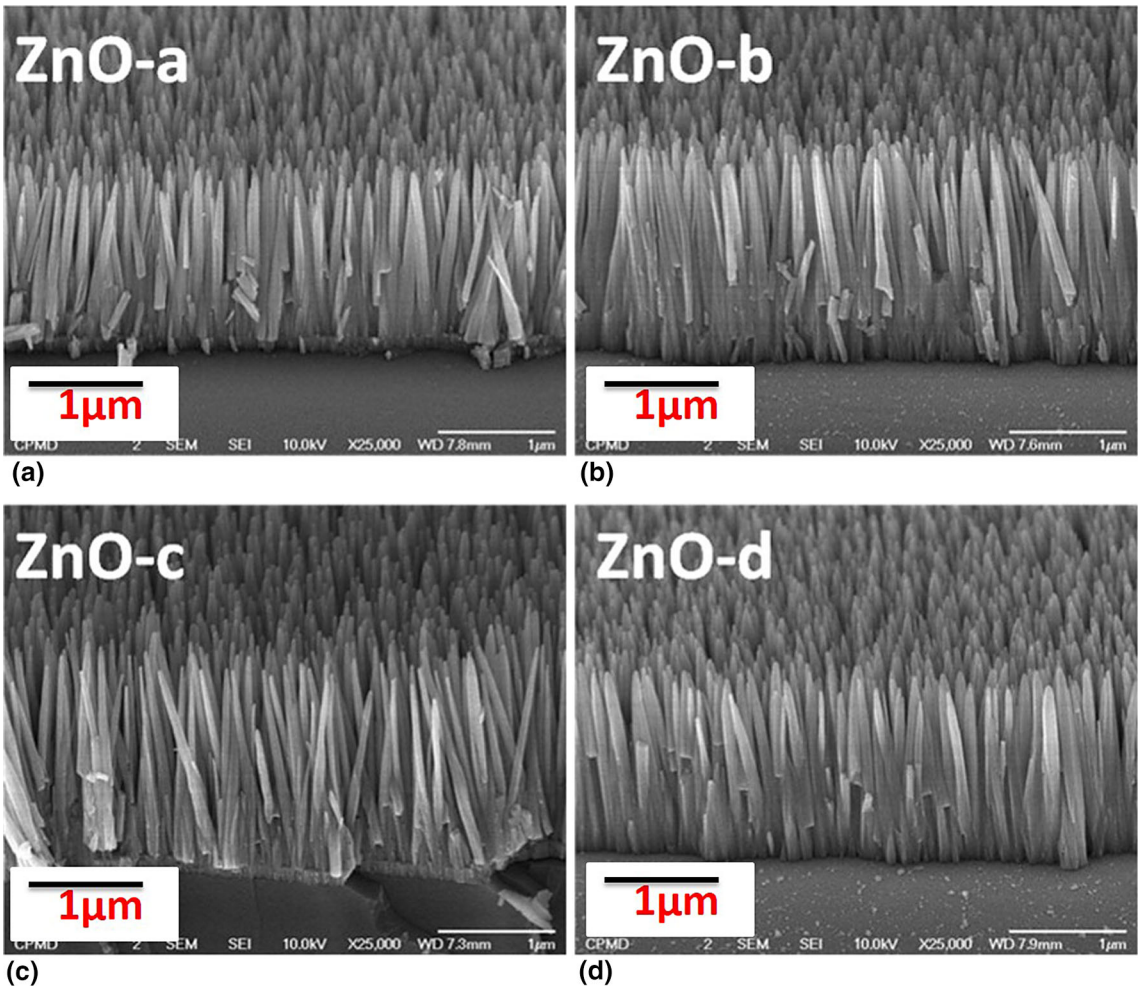

Fig. 3. FESEM images of hydrothermally grown ZnO thin film samples: (a) ZnO-a (b) ZnO-b (c) ZnO-c, and (d) ZnO-d.

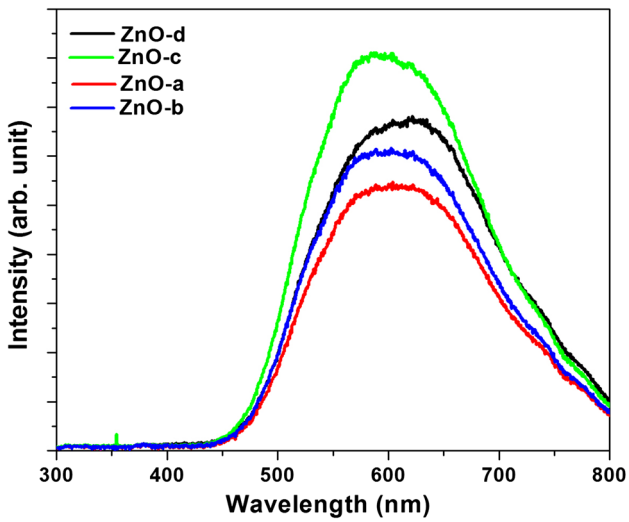

Fig. 4. PL spectra of all ZnO thin films.

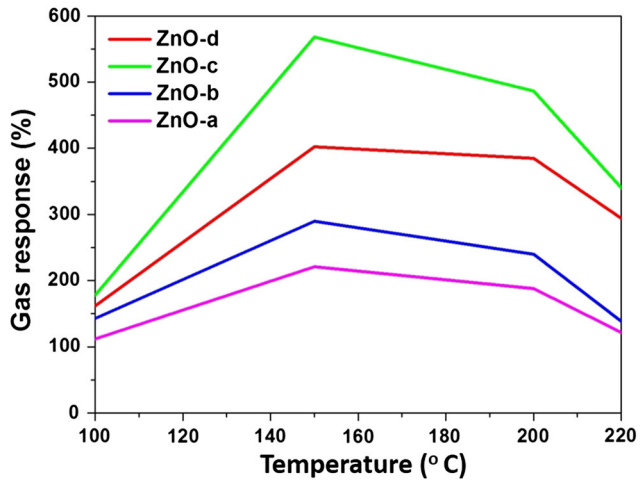

Fig. 5. Variation of gas sensor response of all ZnO thin film samples for 100 ppm of NO_2 gas at different operating temperatures.

NO gas.[31] Meanwhile, Fig. 5 also demonstrates the variation of gas response with respect to the ZnO thin films synthesized at different zinc nitrate concentrations. Samples ZnO-a, ZnO-b, ZnO-c, and ZnO-d show a maximum gas response of about 220, 290, 560, and 400 at 150°C for 100 ppm of NO_2 gas, respectively. Due to the higher gas response observed for sample ZnO-c, it was chosen for the

further gas-sensing study. From Fig. 5, it is concluded that the optimal working temperature is 150°C and the most suitable ZnO sample is ZnO-c. In the meantime, the better gas response observed for sample ZnO-c is the harmonious effect of the higher nanorod length, large surface area, adequate inter-rod spacing, and higher defect density.

Figure 6 shows the variation in electrical resistance of sample ZnO-c when exposed to 100 ppm of NO_2 gas, and Fig. 7 reveals the sensitivity, selectivity, and stability of sample ZnO-c towards NO_2 gas at 150°C. In the gas-sensing measurements, the baseline resistance was obtained under dry air flow. After the stabilization/baseline condition was met, the NO_2 gas was injected so that the resistance of the ZnO-based gas sensor increased and became saturated when all active sites were occupied by gas molecules, as shown in Fig. 6. After the saturation, when the NO_2 gas was removed with dry air, the resistance of ZnO-based gas sensor decreased and reached the original value. In addition, Fig. 6 shows faster responses than their recovery. Figure 7a shows increases in the sensor response to the increase in the NO_2 gas concentration, which may be due to availability of more NO_2 molecules that react with the ZnO sensor surface. The gas response was observed around 15–5 ppm of NO_2 gas, 40–10 ppm, and 560–100 ppm of NO_2 gas. The gas response increased with the concentration, which is helpful if these films are to be used in a digitized sensor. Meanwhile, Fig. 7b shows sensing transient curves of sample ZnO-c for different concentrations of NO_2 gas. In addition, Fig. 7b shows the response and recovery time of sample ZnO-c at different NO_2 gas concentration. The response time for all gas concentrations remains nearly the same; however, the recovery time increases further with increasing gas concentration up to 60 ppm. Interestingly, with further increase in the gas concentration, the recovery time was lowered. This behavior may be attributed to the fast removal of gas species at higher concentration. It is well-known fact that the response time decreases and recovery time increases as the gas concentration is increased. However, the response and recovery times may saturate at the higher gas concentration.[32] Along with operating temperature and gas response, the specific gas selectivity is also a very important feature of a gas sensor. Therefore, the selectivity of sample ZnO-c for 100 ppm of liquefied petroleum gas (LPG) and NO_2 gas is also studied at an operating temperature of 150°C. The ZnO-c-based gas sensor shows a gas response of about 10 and 560 towards 100 ppm of LPG and NO_2 gas, respectively. The selectivity coefficient factor for sample ZnO-c is found to be 56. This high value shows the superior selective nature of our ZnO-based gas sensor towards NO_2 gas as compared to LPG. In addition to LPG, our ZnO-based gas sensor showed a superior gas response towards NO_2 gas as compared to acetone, carbon dioxide (CO_2), hydrogen sulfide (H_2S), and ammonia (NH_3). Figure 7c shows the selectivity of the ZnO gas sensor towards NO_2 gas. Gas responses of about 36, 6, 15, 570, 48, and 10 are observed for the gases such as acetone, CO_2, H_2S, NO_2, NH_3, and LPG, respectively. Moreover, our ZnO-based gas sensor shows enhanced gas response as compared to earlier reports.[23,33–35] In addition to the gas response and specific selectivity, the stability of a gas sensor is an important evaluating factor. Therefore, the stability of ZnO-based gas sensor was studied for 15 days. Figure 7d shows the sensor stability curve of the ZnO gas sensor. It is observed that the gas response of the ZnO thin film sensor remains nearly constant over 15 days of exposure. A minor reduction in the gas response over the period of 15 days is observed and it is ascribed to the formation of a moisture or oxide layer.[36]

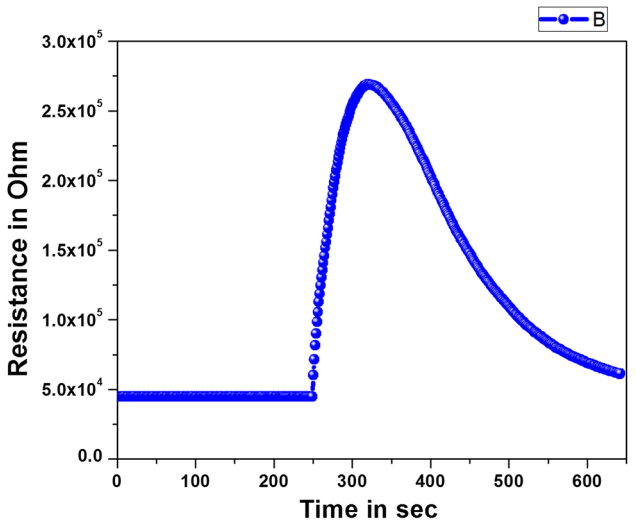

Fig. 6. The variation of electrical resistance of sample ZnO-c when exposed to 100 ppm of NO_2 gas at temperature of 150°C.

In order to explain the enhancement in the NO_2 sensing performance of sample ZnO-c, the gas-sensing mechanism was taken into consideration. In metal oxide gas sensors, the electrical resistance is altered by the interaction of gas molecules. In our case, the interaction of gases with ZnO nanorods includes two steps: adsorption of oxygen molecules from the environment on the surface of nanorods and reaction of adsorbed oxygen ions with NO_2. In the first step, oxygen is physisorbed on the surface of ZnO due to exposure to air. Further, at a high temperature, the chemisorption of oxygen will happen on the ZnO surface. The chemisorbed oxygen molecules trap electrons from the conduction band of the ZnO. Such trapping of electrons leads to increase in the resistance of ZnO. During the second step, the surface of ZnO nanorod is exposed to NO_2 gas. Due to the oxidizing nature, the NO_2 molecule reacts with the chemisorbed oxygen onto the ZnO surface and traps electrons from its conduction band and, in turn, leads to the further increase in the resistance. In addition, the enhancement of the gas-

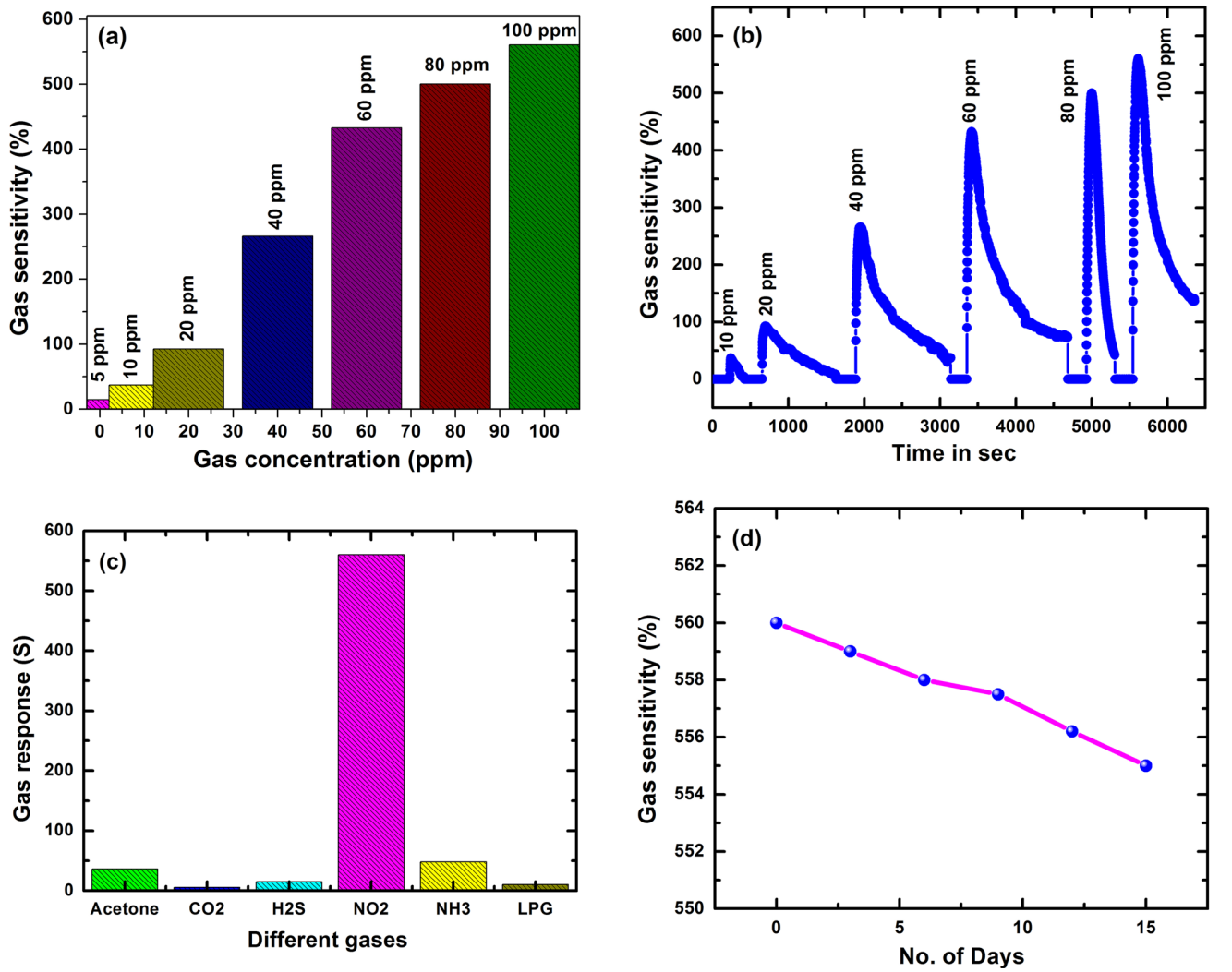

Fig. 7. (a) Gas sensing performance of sample ZnO-c for different ppm of NO_2 gas at the operating temperature 150°C, (b) gas-sensing transient curves of sample ZnO-c for different ppm of NO_2 gas, (c) selectivity nature of sample ZnO-c towards 100 ppm of various target gases, and (d) gas response as a function of time for sample ZnO-c in 100 ppm of NO_2 gas at 150°C.

sensing activity of the ZnO nanorods was controlled by the gas diffusion activity with an efficient surface area. Regular arrangement and proper spacing in adjacent nanorods of sample ZnO-c provides a higher surface area and various tracks for gas diffusion. Since using FESEM images, it is understandable that the length and interspace distance of the nanorods increased when the concentration of the Zn ion precursor is increased. Sample ZnO-d gives less surface area for the gas diffusion as compared to sample ZnO-c. This results in a difficulty for the gas molecule to extent the bottommost and, hence, the recorded gas response was low. Because of the steady and well-set apart ZnO nanorods, sample ZnO-c has a higher effective surface area and defects compared to the other samples and it provides a more reactive surface area along with frequent channels for gas diffusion.

CONCLUSION

In this work, nanorod-like ZnO thin films were prepared using a simplistic hydrothermal route on soda lime glass substrates. The physicochemical properties of the as-synthesized ZnO thin films were investigated with the various characterization techniques mentioned. For all ZnO thin film samples, the broad PL peak appears at < 600 nm, ascribed to the presence of defects such as the oxygen vacancies and interstitial sites. The presences of higher oxygen vacancies are beneficial for the gas-sensing performance of ZnO thin films. Therefore, the as-synthesized ZnO thin films were used to detect dangerous NO_2 gas. The ZnO-based gas sensor shows a gas response of about 570 towards 100 ppm of NO_2 gas at 150°C. Along with the enhanced gas response, the ZnO-based gas sensor shows better selectivity. The improved gas response

observed for sample ZnO-c is the harmonious effect of the higher nanorod length, large surface area, adequate inter-rod space, and the presence of defects.

ACKNOWLEDGMENTS

This work was supported by the Human Resources Development Program (no. 20164030201310) of the Korea Institute of Energy Technology Evaluation and Planning (KETEP) funded by the Korea Government Ministry of Trade, Industry and Energy. This research is partially funded under the project entitled 'Synthesis and characterization of nanostructured metal oxides for gas sensor applications' (No. SR/FTP/PS-083/2012) with a grant from the Science and Engineering Research Board (SERB), Department of Science and Technology (DST), New Delhi, India.

REFERENCES

1. G. Lawrence, P. Kalimuthu, M. Benzigar, K.J. Shelat, K.S. Lakhi, D.-H. Park, Q. Ji, K. Ariga, P.V. Bernhardt, and A. Vinu, *Adv. Mater.* 29, 1702295 (2017).
2. K. Hanabusa, S. Takata, M. Fujisaki, Y. Nomura, and M. Suzuki, *Bull. Chem. Soc. Jpn.* 89, 1391 (2016).
3. I. Osica, G. Imamura, K. Shiba, Q. Ji, L.K. Shrestha, J.P. Hill, K.J. Kurzydłowski, G. Yoshikawa, K. Ariga, and A.C.S. Appl, *Mater. Interfaces* 9, 9945 (2017).
4. S. Yang, C. Jiang, and S. Wei, *Appl. Phys. Rev.* 4, 021304 (2017).
5. S.P. Patil, V.L. Patil, S.S. Shendage, N.S. Harale, S.A. Vanalakar, J.H. Kim, and P.S. Patil, *Ceram. Int.* 42, 16160 (2016).
6. S.B. Jagadale, V.L. Patil, S.A. Vanalakar, P.S. Patil, and H.P. Deshmukh, *Ceram. Int.* 44, 3333 (2018).
7. C. Wang, L. Yin, L. Zhang, D. Xiang, and R. Gao, *Sensors* 10, 2088 (2010).
8. S. Das and V. Jayaraman, *Prog. Mater. Sci.* 66, 112 (2014).
9. S.S. Shendage, V.L. Patil, S.A. Vanalakar, S.P. Patil, N.S. Harale, J.L. Bhosale, J.H. Kim, and P.S. Patil, *Sens. Actuators B Chem.* 240, 426 (2017).
10. S.A. Vanalakar, V.L. Patil, N.S. Harale, S.A. Vhanalakar, M.G. Gang, J.Y. Kim, P.S. Patil, and J.H. Kim, *Sens. Actuators B Chem.* 221, 1195 (2015).
11. A. Menzel, K. Subannajui, F. Güder, D. Moser, O. Paul, and M. Zacharias, *Adv. Funct. Mater.* 21, 4342 (2011).
12. E. Fortunato, A. Gonçalves, A. Pimentel, P. Barquinha, G. Gonçalves, L. Pereira, I. Ferreira, and R. Martins, *Appl. Phys. A* 96, 197 (2009).
13. S.A. Vanalakar, R.C. Pawar, M.P. Suryawanshi, S.S. Mali, D.S. Dalavi, A.V. Moholkar, K.U. Sim, Y.B. Kown, J.H. Kim, and P.S. Patil, *Mater. Lett.* 65, 548 (2011).
14. S.A. Vanalakar, S.S. Mali, R.C. Pawar, D.S. Dalavi, A.V. Mohalkar, H.P. Deshamukh, and P.S. Patil, *Ceram. Int.* 38, 6461 (2012).
15. R. Kumar, O.A. Dossary, G. Kumar, and A. Umar, *Nano-Micro Lett.* 7, 97 (2015).
16. V.L. Patil, S.S. Kumbhar, S.A. Vanalakar, N.L. Tarwal, S.S. Mali, J.H. Kim, and P.S. Patil, *New J. Chem.* 42, 13573 (2018).
17. A.N. Afaah, Z. Khusaimi, and M. Rusop, *Adv. Mater. Res.* 667, 329 (2013).
18. A.I. Hochbaum and P. Yang, *Chem. Rev.* 110, 527 (2010).
19. S.A. Phaltane, S.A. Vanalakar, T.S. Bhat, P.S. Patil, S.D. Sartale, and L.D. Kadam, *J. Mater. Sci. Mater. Electron.* 28, 8186 (2017).
20. P.N. Bhosale, V.V. Kondalkar, R.M. Mane, S. Choudhury, and K.V. Khot, *J. Nanomed. Nanotechnol.* 6, 1 (2015).
21. S.A. Vanalakar, G.L. Agwane, M.G. Gang, P.S. Patil, J.H. Kim, and J.Y. Kim, *Phys. Status Solidi C* 12, 500 (2015).
22. Y.B. Kwon, S.W. Shin, H.K. Lee, J.Y. Lee, J.H. Moon, and J.H. Kim, *Curr. Appl. Phys.* 11, 197 (2011).
23. K.V. Gurav, M.G. Gang, S.W. Shin, U.M. Patil, P.R. Deshmukh, G.L. Agawane, M.P. Suryawanshi, S.M. Pawar, P.S. Patil, C.D. Lokhande, and J.H. Kim, *Sens. Actuators B Chem.* 190, 439 (2014).
24. L.E. Greene, M. Law, D.H. Tan, M. Montano, J. Goldberger, G. Somorjai, and P. Yang, *Nano Lett.* 5, 1231 (2005).
25. N. Qin, Q. Xiang, H. Zhao, J. Zhang, and J. Xu, *CrystEngComm* 16, 7062 (2014).
26. S.A. Vanalakar, S.S. Mali, M.P. Suryawanshi, N.L. Tarwal, P.R. Jadhav, G.L. Agawane, K.V. Gurav, A.S. Kamble, S.W. Shin, A.V. Moholkar, J.Y. Kim, J.H. Kim, and P.S. Patil, *Opt. Mater.* 37, 766 (2014).
27. C. Tsakonas, W. Cranton, F. Li, K. Abusabee, and A. Flewitt, *J. Phys. D Appl. Phys.* 46, 095305 (2013).
28. J.H. Lin, R.A. Patil, R.S. Devan, Z.A. Liu, Y.P. Wang, C.H. Ho, Y. Liou, and Y.R. Ma, *Sci. Rep.* 4, 6967 (2014).
29. N.L. Tarwal, P.R. Jadhav, S.A. Vanalakar, S.S. Kalagi, R.C. Pawar, J.S. Shaikh, S.S. Mali, D.S. Dalavi, P.S. Shinde, and P.S. Patil, *Powder Technol.* 208, 185 (2011).
30. V.L. Patil, S.A. Vanalakar, A.S. Kamble, S.S. Shendage, J.H. Kim, and P.S. Patil, *RSC Adv.* 6, 90916 (2016).
31. A. Sharma, M. Tomar, and V. Gupta, *Sens. Actuators B Chem.* 156, 743 (2011).
32. V.N. Mishra and P. Agarwal, *Microelectron. J.* 29, 861 (1998).
33. S.K. Shaikh, V.V. Ganbavle, S.I. Inamdar, and K.Y. Rajpure, *RSC Adv.* 6, 25641 (2016).
34. X. Wang, F. Sun, Y. Duan, Z. Yin, W. Luo, Y. Huang, and J. Chen, *J. Mater. Chem. C* 3, 11397 (2015).
35. P. Rai, Y.S. Kim, H.M. Song, M.K. Song, and Y.T. Yu, *Sens. Actuators B Chem.* 165, 133 (2012).
36. V.L. Patil, S.A. Vanalakar, P.S. Patil, and J.H. Kim, *Sens. Actuators B Chem.* 239, 1185 (2017).